3

4 **New nanoadsorbent based on magnetic iron oxide containing**

5 **1,4,7,10-tetraazacyclododecane in outer chain (Fe$_3$O$_4$@SiO$_2$-cyclen) for**

6 **adsorption and removal of selected heavy metal ions Cd^{2+}, Pb^{2+}, Cu^{2+}**

7

8 **Amanda Kulpa-Koterwa[a], Jacek Ryl[b], Karolina Górnicka[c], Paweł Niedziałkowski[a,*]**

9

10

11 [a] Department of Analytical Chemistry, Faculty of Chemistry, University of Gdansk, Wita Stwosza 63, 80-308 Gdańsk, Poland

12

13 [b] Division of Electrochemistry and Surface Physical Chemistry, Institute of Nanotechnology and Materials Engineering and Advanced Materials Center, Gdańsk University of Technology, Narutowicza 11/12, 80-233 Gdańsk, Poland

14

15 [c] Faculty of Applied Physics and Mathematics, Advanced Materials Center, Gdansk University of Technology, Narutowicza 11/12, 80-233 Gdansk, Poland

16

17

*corresponding author: Paweł Niedziałkowski

e-mail address: pawel.niedzialkowski@ug.edu.pl

18 **Abstract**

19 Magnetic $Fe_3O_4@SiO_2$-cyclen nanoparticles were prepared and used as adsorbent for Cd^{2+},

20 Pb^{2+} and Cu^{2+} from aqueous solution removal process controlled with differential pulse anodic

21 stripping voltammetry (DPASV) and hanging mercury drop electrode (HDME). Nanomaterial

22 was synthesised in three-step process co-precipitation of Fe_3O_4 core, coating with silane and N-

23 (3-(triethoxysilyl)propyl)-1,4,7,10-tetraazacyclododecane-1-carboxamide   silane

24 functionalisation. The effectiveness of each step of the synthesis was confirmed using scanning

25 electron microscopy (SEM), high-resolution X-ray photoelectron spectroscopy (XPS), powder

26 X-ray diffraction (pXRD) and fourier-transform infrared spectroscopy (FT-IR) techniques. The

27 $Fe_3O_4@SiO_2$-cyclen nanoparticles were employed for Cd^{2+}, Pb^{2+} and Cu^{2+} ions elimination

28 from individual and mixed solutions by carrying out titration with a suspension of

29 nanocomposites. The binding level for all ions both in the individual solutions and in the

30 mixture was very similar at high levels. For Cd^{2+} and Cu^{2+} ions sorption efficiency level was

31 from 83% to 89%, while for Pb^{2+} ions it was slightly lower at the level over 73%. In all cases,

32 the equilibrium adsorption capacity parameter was over 1 mg/g and reached definitely higher

33 values for individual ions solutions. The research results revealed that $Fe_3O_4@SiO_2$- cyclen

34 nanoparticles can be a promising adsorbent for magnetic heavy metal ions water treatment

35 agents.

36

37 **Keywords:** functionalised Fe_3O_4 nanoparticles, stripping voltammetry, Cd^{2+}, Pb^{2+} and Cu^{2+}

38 ions binding, nanoadsorbent, 1,4,7,10-tetraazacyclododecane, heavy metal ions removal

39 **Highlights**

40 • $Fe_3O_4@SiO_2$- cyclen nanoparticles was utilised for the removal of Cd^{2+}, Pb^{2+}, Cu^{2+}.

41 • The SEM, XPS, pXRD and FT-IR characterisation of nanoparticles was performed.

42 • Ions binding kinetics and efficiency were investigated with DPASV and HDME.

43 • Sorption efficiency was calculated and reached a maximum level of nearly 90%.

44 • The effectiveness of ions magnetic separation from the aqueous solution was confirmed.

45

1. Introduction

Over the last few decades, a significant increase has been observed in environmental pollution with heavy metal ions, which is a problem all over the world [1]. The increasing heavy metal ions concentration is generated mainly by technological and operational activities, production processes such as refining, power plants and combined heat and power plants, steel mills, coal and waste combustion, the chemical industry, the use of fertilisers and pesticides, and transport [2]. The presence of heavy metal ions in the environment constitutes a threat due to the possibility of their migration along the rungs of the trophic chain from soil, air, surface waters to plants, animals and in consequence to humans. Exposure to continuously increasing heavy metal ions concentrations lowers the action of biological barriers, which has a negative impact on human health due to their low biodegradability, bioaccumulation tendency, potential carcinogenic effect and mutagenicity [3]. Due to the danger posed by heavy metal ions environment contamination, the recycling of them from aquatic environments has become a very important area of scientific research and industry.

Until now, many methods of metal ions remediation from the environment have been used [4,5], particularly methods such as membrane filtration [6], osmosis [7], ion exchange [8], extraction with ionic liquids [9], photocatalysts [10], clays/layered double hydroxides [11], bioremediation [12], biomass and biosorption [13] phytoremediation [14], precipitation and coagulation [15,16] or electrocoagulation [17]. The conventional wastewater treatment technologies involving physical, chemical, and biological methods have their advantages but also disadvantages such as high costs, complex working operation, secondary pollutants production, low selectivity and many others [18]. To overcome these challenges, researchers used adsorption process as an alternative due to its wide working potentials, low price, simplicity in use, process efficiency, selectivity, capacity for material regeneration and pollutants trace concentration removal [19,20]. A wide range of materials have found application as heavy metal ions adsorbents e.g., chitosan and its functionalised forms [21], aerogels and their derivatives [22], based on cellulose [23], metal organic frameworks [24], carbon-based materials [25], polymers [26], dendrimers [27] and many others [28–31]. However, among many research groups, various nanoscale adsorbents became very popular due to their high surface area, high mobility in solution, reactivity, good adsorption capacity and in consequence efficiency [32]. A series of nanoparticles and their modification were investigated as heavy metal adsorbents but, in recent years, a particular interest was attached to nanoparticles with magnetic properties, especially magnetite Fe_3O_4 [33,34]. Magnetite

79 nanoparticles occupy a special importance due to the possibility of easy and quick isolation

80 with the use of an external magnetic field [35]. Furthermore, creating core-shell type structures

81 with silica $Fe_3O_4@SiO_2$ provides a good basis for further functionalisation thus for obtaining a

82 material with wide applicability and selectivity [36–38]. There are known plenty of

83 $Fe_3O_4@SiO_2$ modified structures for heavy metal ions adsorption, however, the search for new

84 and selective composites is still topical [39–41]. So far, there is lack of knowledge about crown

85 ethers usage as surface nanocomposites modifiers. Qin et al. designed and synthesised silica gel

86 bound di(aminobenzo)-18-crown-6(SGN18) for zirconium and hafnium adsorption [42]. Aza-

87 crown ethers and derivatives in their heyday were widely used as complexation agents of metal

88 ions in wide range of applications [43,44]. One of the well-known and widely used agent as a

89 metal ions complexation was 1,4,7,10-tetraazacyclododecane [45–49].

90   In view of the fact that previously the authors used $Fe_3O_4@SiO_2$ nanoparticles

91 containing nitrogen atoms in the outer chain as heavy metal ion adsorbent [50,51], they now

92 decided to combine the excellent complexing properties of 1,4,7,10-tetraazacyclododecane and

93 the possibility of pollutants magnetic isolation. In this work, magnetic core-shell nanoparticles

94 functionalised with 1,4,7,10-tetraazacyclododecane $Fe_3O_4@SiO_2$-cyclen were designed,

95 synthesised and used as heavy metal Cd^{2+}, Pb^{2+}, and Cd^{2+} ions adsorbent for the first time. The

96 newly obtained nanomaterial was characterised at every stage of synthesis using SEM, FT-IR,

97 pXRD and (XPS) methods. Furthermore, the ions binding kinetics studies was performed and

98 the binding capacity of nanoparticles was investigated using the differential pulse anodic

99 stripping voltammetry (DPASV) method coupled with hanging mercury drop electrode (HDM)

100 electrode. It is worth mentioning that the application of electrochemical detection skips

101 conventional techniques' limitations in heavy metal detection and offers the same sensitivity

102 with a lower cost, less complex operational procedures and fast on-site detection [52].

103

104 **2. Experimental**

105 **2.1. Reagents**

106   All analytical grade reagents were purchased from the indicated suppliers and used

107 without further purification. All inorganic salts – ferric chloride hexahydrate ($FeCl_3 \cdot 6H_2O$),

108 ferrous chloride tetrahydrate ($FeCl_2 \cdot 4H_2O$), potassium chloride KCl (99.9%), cadmium nitrate

109 tetrahydrate $Cd(NO_3)_2 \cdot 4H_2O$ (99.9%), lead nitrate $Pb(NO_3)_2$, and copper nitrate trihydrate

110 $Cu(NO_3)_2 \cdot 3H_2O$ (99.9%) – were purchased from POCh (Poland). The organic solvents,

111 ammonia (25%), tetraethylorthosilicate (98%) (TEOS), triethoxy(3-isocyanatopropyl)silane

112   were purchased from Sigma-Aldrich (Poland). 1,4,7,10-tetraazacyclododecane was bought

113   from Strem Chemicals. Aqueous solutions were prepared using ultra-pure deionised water.

2.2. Synthesis of core-shell $Fe_3O_4@SiO_2$-cyclen nanostructures

115   New functionalised nanocomposites were obtained in the three-steps synthesis process.

116   In the first stage, a magnetic Fe_3O_4 core was received by the co-precipitation method. The

117   mixture of $Fe^{2+}(FeCl_2 \cdot 4H_2O)$ and Fe^{3+} ($FeCl_3 \cdot 6H_2O$) in aqueous solution using a three-neck

118   flask was stirred under nitrogen conditions. Then the 25% ammonia solution was dripped into

119   the reaction until the pH reached 11. Then the reaction mixture was heated to 60 °C for 3 hours

120   to complete precipitation of the magnetite. The obtained nanoparticles were separated by a

121   magnet and washed with distilled water several times.

122   The second stage of the synthesis involved the nanomagnetite coating with silica

123   forming $Fe_3O_4@SiO_2$, which was used for further modification. 16 g of Fe_3O_4 nanoparticles

124   obtained in the previous stage was dispersed in a mixture of 240 mL EtOH and 60 ml H_2O.

125   Then 3 mL of TEOS was added into reaction and the reaction was heated overnight to 50 °C.

126   After this time, the obtained nanoparticles were magnetically collected and washed with

127   distilled water several times.

128   In next stage of synthesis it was necessary to synthesise a modifier of the obtained

129   nanoparticles $Fe_3O_4@SiO_2$ due to the fact that the silane derivatives containing 1,4,7,10-

130   tetraazacyclododecane are not a commercially available.

131   The reaction of 1,4,7,10-tetraazacyclododecane with triethoxy(3-

132   isocyanatopropyl)silane was performed according to the modified procedure described

133   previously [53] to obtain N-(3-(triethoxysilyl)propyl)-1,4,7,10-tetraazacyclododecane-1-

134   carboxamide.

135   To the solution of 1,4,7,10-tetraazacyclododecane (4.179 g, 24,256 mmol) dissolved in

136   200 ml dichloromethane 6 mL of triethoxy(3-isocyanatopropyl)silane (24,256 mmol) was

137   dropwise added and the reaction was carried out overnight at 40 °C under a reflux condenser.

138   Then the solvent was evaporated under reduced pressure. The obtained colourless oil was dried

139   in a vacuum desiccator over P_2O_5 to obtain 2.159 g of colourless solid with a yield of 21.33%.

140   MALDI-TOF MS: m/z 419,29 $[M+H]^+$, (MW = 420.31).

141   IR (KBr) (cm^{-1}): 3291, 2972, 2926, 2886, 2735, 1627, 1536, 1478, 1444, 1391, 1365, 1254,

142   1189, 1165, 1103, 1078, 955, 784.

143   ^{1}H-NMR (CDCl$_3$): 0.538-0.572 (t, 2H, (CH$_3$-CH$_2$)$_3$SiO-<u>CH$_2$</u>-CH$_2$-CH$_2$-HN-, J_1 = 7 Hz;

144   J_1 = 10,0 Hz; J_2=8,5 Hz); 1.135-1.165 (dt, 9H, (<u>CH$_3$</u>-CH$_2$)$_3$SiO-CH$_2$-CH$_2$-CH$_2$-HN-, J_1=1 Hz;

145     $J_1 = 1,5$ Hz; $J_1 = J_2 = 7.0$ Hz); 1.479-1.623 (m, 2H, (CH$_3$-CH$_2$)$_3$SiO-CH$_2$-<u>CH$_2$</u>-CH$_2$-HN-);

146   2.564-3.652 (m, 18H, (CH$_3$-CH$_2$)$_3$SiO-CH$_2$-CH$_2$-<u>CH$_2$</u>-HN- -H-<u>CH$_2$</u>-<u>CH$_2$</u>-N-,); 3.734-3.754 (q,

147   6H, (CH$_3$-<u>CH$_2$</u>)$_3$SiO-CH$_2$-CH$_2$-CH$_2$-HN-, J_1=3 Hz; $J_1 = 4$ Hz; $J_3 = J_4 = 3.0$ Hz);

148

149   The third stage consisted of Fe$_3$O$_4$@SiO$_2$ modification to obtain Fe$_3$O$_4$@SiO$_2$-cyclen.

150   1.593 g of Fe$_3$O$_4$@SiO$_2$ was added to a solution of (3.324 g, 7,928 mmol) N-(3-

151   (triethoxysilyl)propyl)-1,4,7,10-tetraazacyclododecane-1-carboxamide dissolved in 150 mL

152   toluene. Then the reaction mixture was stirred for 12 h at 120 °C. After cooling to room

153   temperature the obtained product was magnetically collected and washed several times with

154   toluene and then with methanol. The resulting product was air-dried.

155
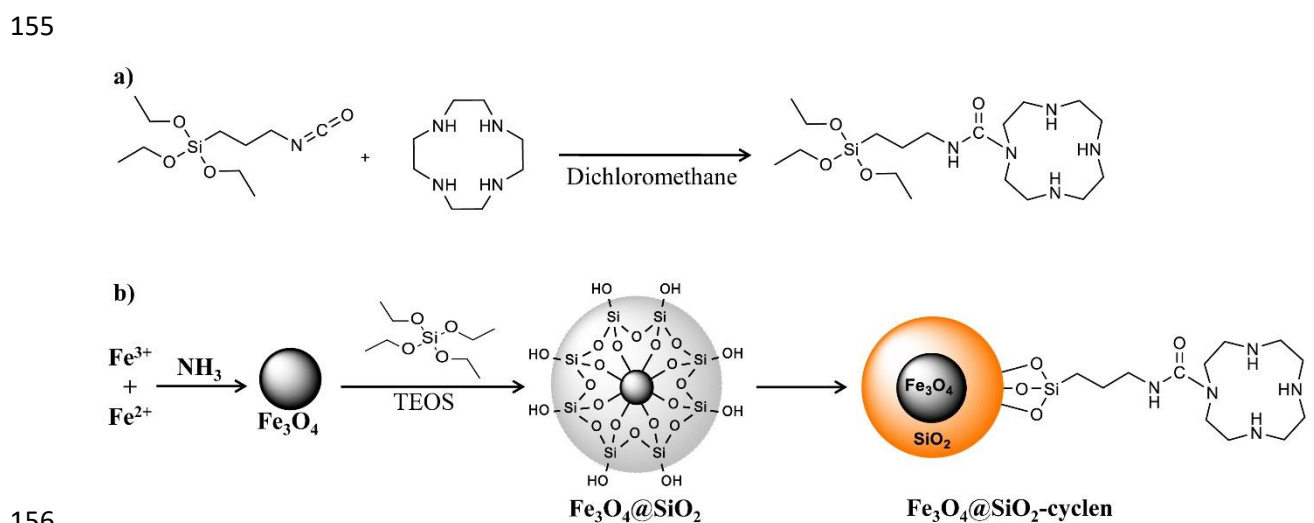
156
157

158   **Figure 1.** Scheme of a) nanoparticles modifier N-(3-(triethoxysilyl)propyl)-1,4,7,10-
159   tetraazacyclododecane-1-carboxamide and b) functionalised Fe$_3$O$_4$@SiO$_2$-cyclen
160   nanocomposite synthesis.

161   **2.3. The Cd^{2+}, Pb^{2+} and Cu^{2+} ions removal experiments from aqueous solutions by**
162   **Fe$_3$O$_4$@SiO$_2$-cyclen binding**

163   The removal experiments of Cd^{2+}, Pb^{2+} and Cu^{2+} ions from aqueous solutions were

164   performed by titration with Fe$_3$O$_4$@SiO$_2$-cyclen nanoparticles. The ions-binding abilities of

165   Fe$_3$O$_4$@SiO$_2$-cyclen were studied in the solutions containing both individual ion or the mixture

166   of Cd^{2+}, Pb^{2+} and Cu^{2+} ions in concentration level $4.5 \cdot 10^{-6}$ M. Before starting (DPASV)

167   measurement a 0.25 mg of Fe$_3$O$_4$@SiO$_2$- cyclen nanoparticles was added into ion solution at

168   each titration step and then mixed for 20 minutes All measurements were performed in 0.5 M

169   KCl pH 6.00.

2.4. Methods

Fourier Transform Infrared Spectroscopy (FT-IR) spectra were obtained were recorded on a Perkin Elmer Spectrum™ 3 FT-IR spectrometer with the KBr pellet technique.

Maldi-Tof mass spectra was performed on autoflex maX Brucker using α-cyano-4-hydroxycinnamic acid (CCA) as a matrix.

^{1}H NMR spectra were recorded in CDCl$_3$ on a Bruker Advance III 500 MHz, where tetramethylsilane (TMS) was used as the internal standard. The chemical shifts are reported in ppm, while the signal patterns are given as follows: triplet (t), doublet of triplets (dt), quartet (q) and multiplet (m).

The scanning electron microscopy (SEM) images were captured with an FEI Quanta 250 FEG (ThermoFisher Scientific) microscope, equipped with a Schottky field emission gun. The microscope was operating at 20 kV accelerating voltage in high vacuum mode.

High-resolution X-ray Photoelectron Spectroscopy (XPS) analysis was carried out using Escalab 250Xi multispectroscope (ThermoFisher Scientific). The spectroscope is equipped with an AlKα x-ray source; the pass energy through the hemispherical analyser was 20 eV. The measurement was assisted with low-energy electron and low-energy Ar$^+$ ion bombardment for charge compensation. The measurements were carried out in C 1s, Fe 2p, Si 2p and N 1s core-level binding energy range, where the adventitious C 1s spectra (284.6 eV) was used for final peak calibration. Peak deconvolution was performed using Avantage v5.9921 (ThermoFisher Scientific).

The crystalline phases and crystallite size were determined by room-temperature powder x-ray diffraction (pXRD). The pXRD patterns were collected on D2 Phaser (Brucker) diffractometer, using CuKα radiation (λ = 1.54056 Å) with a scanning angle 2θ = 5–90° and a step size 0.01°. LeBail refinement of the pXRD pattern was performed to determine the lattice parameters, using the DIFFRAC.SUITE TOPAS.

All differential pulse anodic stripping voltammetry (DPASV) measurements were performed using an Autolab potentiostat/galvanostat (PGSTAT-128N, Methrom), equipped with NOVA 2.1.4 software. Three electrode Teflon electrochemical cell was used in all experiments to avoid metal ions sorption on the glass surface. A Static Drop Mercury Electrode (SDME) 663 VA Stand Metrohm was used as a working electrode. The reference electrode was calomel electrode Hg|Hg$_2$Cl$_2$|KCl$_{(saturated)}$ and platinum wire (Pt) were used as the counter electrode.

202   The detection of Cd^{2+}, Pb^{2+}, and Cd^{2+} by DPASV method was performed using the
203   following conditions: deposition time 90 s, deposition potential –0.9 V, modulation amplitude
204   0.05 V, modulation time 0.07 s, interval time 1.85 s, and step potential 0.003 V. The
205   simultaneous Cd^{2+}, Pb^{2+}, and Cd^{2+} ions was performed in a potential range of –0.8 V to –0.04
206   V, while the individual detection of ions was performed in potential range of –0,8 V to –0.5 V,
207   – 0,6 V to –0.3 V and –0,4 V to –0.04 V for Cd^{2+}, Pb^{2+}, Cu^{2+} detection, respectively.

208   The metal ions solutions were prepared in the supporting electrolyte, which was
209   potassium chloride KCl 0.5 M, pH 6.0. The $Fe_3O_4@SiO_2$-cyclen nanoparticles suspension in
210   supporting electrolyte solution before each measurement was freshly prepared by using
211   ultrasonic bath for 30 minutes.

212

213   **3. Results and discussion**

214   **3.1. XPS and SEM analysis**

215   The high-resolution XPS analysis was performed to evaluate the efficiency of
216   consecutive Fe_3O_4 nanoparticles functionalisation steps. The XPS spectra of each studied
217   sample are presented in Fig. 2.
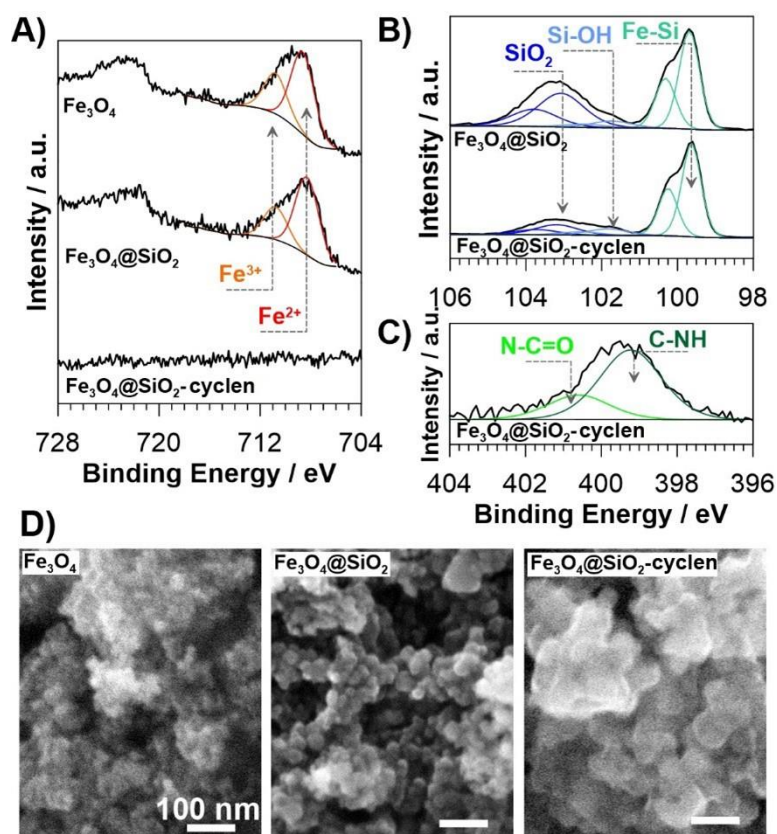
218

219 **Figure 2.** High-resolution XPS analysis of the studied Fe_3O_4, $Fe_3O_4@SiO_2$ and
220 $Fe_3O_4@SiO_2$- cyclen samples in the binding energy range of: A) Fe 2p, B) Si 2p and C) N 1s
221 peak with spectral deconvolution. D) SEM micrographs of studied materials. The scale bar
222 marks 100 nm.

223 Figure 2A shows iron chemistry. The spectra obtained for the Fe_3O_4 sample may be
224 deconvoluted into two Fe $2p_{3/2}$ features, peaking at 708.6 and 710.8 eV, which is characteristic
225 of Fe^{2+} and Fe^{3+} in Fe_3O_4, respectively [54]. The calculated $Fe^{2+}:Fe^{3+}$ ratio is 2:1. Importantly,
226 upon the formation of $Fe_3O_4@SiO_2$ core-shell structure, the peak position as well as the
227 $Fe^{2+}:Fe^{3+}$ ratio remains unchanged, testifying to unchanged iron chemistry and structure within
228 the nanoparticles. Nevertheless, the Fe 2p spectra intensity weakens upon the NP coverage with
229 an SiO_2 shell, and eventually becomes indistinguishable for $Fe_3O_4@SiO_2$-cyclen, due to the
230 limited depth of the XPS signal origin (approx. 3-5 nm).

231 The Si 2p spectra shows more complex character, with not less than three deconvolution
232 peak doublets to be distinguished in Figure 2B. The characteristic component at 103.2 eV is
233 attributed to SiO_2 while the second, smaller component negatively shifted at 0.9 eV may
234 correspond to Si-OH bonds [55]. The third, notable component with Si $2p_{3/2}$ at 99.8 eV may
235 have multiple origins, including Si-Fe bonds [56] or even Si-C bonds [57]. Adventitious carbon
236 contribution in $Fe_3O_4@SiO_2$ NP powder is a relevant source for Si-C. After further modification
237 with N-(3-(triethoxysilyl)propyl)-1,4,7,10-tetraazacyclododecane-1-carboxamide the share of
238 99.8 eV feature rises by 35%. This modification is assisted with two time decreases of the SiO_2
239 share, again due to the restricted depth of the XPS analysis. The detailed information are
240 presented in **Table 1**.

241

242 **Table 1.** The chemical composition (in at.%) using XPS analysis by peak deconvolution.

| Sample	Fe 2p		Si 2p			N 1s	
	Fe^{2+}	Fe^{3+}	SiO_2	Si-OH	Si-(Fe/C)	NH-C	NC=O
BE / eV	708.6	710.8	103.2	102.3	99.8	399.3	400.6
Fe_3O_4	67.1	32.9	--	--	--	--	--
$Fe_3O_4@SiO_2$	1.3	0.6	40.2	6.9	50.0	--	--
$Fe_3O_4@SiO_2$-cyclen	--	--	16.4	9.7	67.4	4.8	1.7

243

244   While the N-(3-(triethoxysilyl)propyl)-1,4,7,10-tetraazacyclododecane-1-carboxamide
245   compounds do not introduce C 1s features that can be easily differentiated from the surface-
246   adsorbed adventitious carbon under air exposure, the successful Fe_3O_4@SiO_2-cyclen synthesis
247   may be confirmed tracking N 1s spectral shape. As seen in Figure 2C this peak was
248   deconvoluted using two separate components. The first, and more notable, at 399.3 eV is
249   characteristic of NH-C bonds [58], while the latter, at 400.6 eV, was assigned to NC=O [59].

250   The morphology of each studied nanomaterial was revealed by SEM micrographs as
251   seen in Figure 2D. The size of the Fe_3O_4 nanoparticles is below 20 nm, thus making it
252   impossible for accurate estimation. Such small particle size is reported as sufficient to achieve
253   superparamagnetism in Fe_3O_4 NPs [60]. Further encapsulation in SiO_2 by TEOS allows for full
254   NP contours to be recognised and increasing the average size to approx. 34 ± 5 nm. This result
255   suggests the SiO_2 thickness to exceed 5 nm, testifying for nearly the entire removal of the high
256   resolution Fe 2p signal. The final functionalisation notably enlarges the Fe_3O_4@SiO_2-cyclen
257   dimensions, which now reach 50 to as much as 100 nm. The less regular size introduced by
258   Sil- Prop- cyclen is the probable explanation behind a significant share of Si still to be
259   recognised by XPS.

260

261   **3.2. pXRD analysis**

262   The pXRD analysis was used to investigate the crystallinity nature, and size of crystallites of
263   bare Fe_3O_4 nanoparticles and after each functionalisation steps. The XRD patterns of a) bare
264   Fe_3O_4, b) silica-coated Fe_3O_4@SiO_2,and c) functionalised Fe_3O_4@SiO_2-cyclen nanoparticles
265   together with the LeBail refinement (solid red line) are presented in Figure 3. A difference
266   plot (between experimental and fitted data) and the Bragg positions are also shown in Figure
267   3.

268
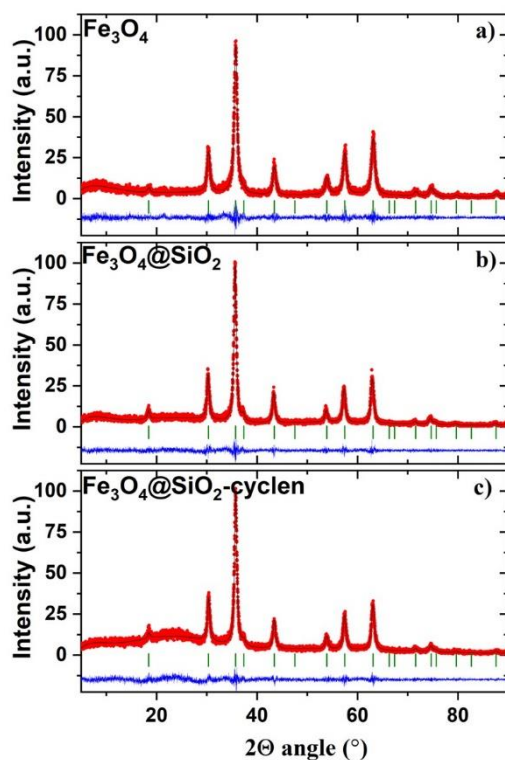
Figure 3. Powder x-ray diffraction pattern (pXRD) (red points) together with the LeBail refinement profile (solid black line) for a) bare Fe_3O_4, b) silica coated $Fe_3O_4@SiO_2$ and c) functionalized $Fe_3O_4@SiO_2$-cyclen. The green vertical bars indicate the expected Bragg peak positions for Fe_3O_4 (JCPDS card PDF 00-065-0731).

Our pXRD analysis confirms that for each studied sample all the diffraction peaks correspond to the cubic crystal structure (space group *Fd-3m*, no. 227). Estimated lattice parameters for the Fe_3O_4 phase do not differ much and are $a = 8.329(1)$ Å for bare Fe_3O_4, $a = 8.3521(6)$ Å for $Fe_3O_4@SiO_2$, and $a = 8.3462(6)$ Å for $Fe_3O_4@SiO_2$-cyclen nanoparticles. The average crystallite size of the Fe_3O_4 phase was estimated from the Scherrer formula based on the line broadening at half the maximum intensity of the reflection (220). The estimated crystallite sizes are 14, 19 and 18 nm for Fe_3O_4, $Fe_3O_4@SiO_2$, and $Fe_3O_4@SiO_2$-cyclen samples, respectively. The obtained results are in agreement with SEM micrographs.

3.3. FT-IR spectroscopy analysis

FT-IR analysis was performed to identify the appropriate functional groups present in the Fe_3O_4 nanoparticles at each functionalisation steps.
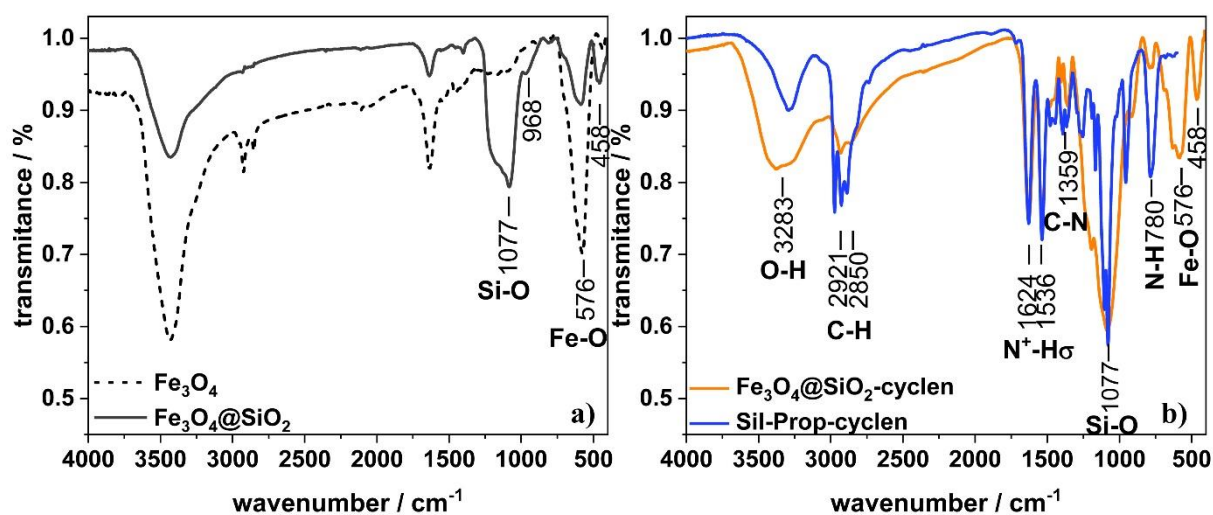
Figure 4. FT-IR spectra for a) bare Fe_3O_4, silica coated $Fe_3O_4@SiO_2$ and b) functionalised $Fe_3O_4@SiO_2$-cyclen nanoparticles, modifier silane N-(3-(triethoxysilyl)propyl)-1,4,7,10-tetraazacyclododecane-1-carboxamide (Sil-Prop-cyclen).

The Fe_3O_4 spectrum (Figure 4 a) shows strong stretching vibration Fe–O band at 576 cm^{-1} typical for iron oxide [61]. Also observed was the reduction in the Fe–O band intensity for coated nanoparticles with silica and functional group. The band intensity decrease confirms the success in the surface functionalisation process [50]. After silica coating of nanomagnetite the intense Si–O band appeared at 1077 cm^{-1}. It is associated with stretching vibrations of Si–O–Si and O–Si–O on the surface of the magnetic core at 968 cm^{-1} and 1077 cm^{-1}, respectively [62,63]. The broad strong band at 3433 cm^{-1} is related to the overlapping of O–H stretching bond, which proves hydroxyl groups formation on the magnetite surface [64]. Figure 4 b blue line shows spectra for nanoparticles modifier N-(3-(triethoxysilyl)propyl)-1,4,7,10-tetraazacyclododecane-1-carboxamide for comparison. A 780 cm^{-1} weak band and a two headed band about 1536 cm^{-1} and 1624 cm^{-1} characteristic for N–H vibrations are observed. Furthermore, there are bands that appeared at 1359 cm^{-1} and about 2900 cm^{-1} corresponding to C–N and N–H stretching vibrations, respectively. The same characteristic bands for the spectrum for the functionalised nanoparticles $Fe_3O_4@SiO_2$-cyclen (Figure 4 b orange line) are observed, which proves the success of the nanomaterials synthesis process. In addition, there is a bandwidth extension at 3283 cm^{-1} which probably corresponds to overlapping O–H and N–H bands. On the basis of SEM, XPS and FT-IR analysis it can be concluded that the functionalised core-shell nanoparticles formation was conducted successfully.

3.3. Electrochemical analysis

In this work, the independent and simultaneous determination of Cd^{2+}, Pb^{2+} and Cu^{2+} ions was performed under optimised experimental conditions using the DPASV method and HDM electrode. 1,4,7,10-tetraazacyclododecane functionalised magnetite nanoparticles $Fe_3O_4@SiO_2$-cyclen were investigated as a new heavy metal ions adsorbent. To examine the ions-binding abilities of $Fe_3O_4@SiO_2$-cyclen, a series of measurements were performed in the solutions containing Cd^{2+}, Pb^{2+} and Cu^{2+} ions in concentration level $4.5 \cdot 10^{-6}$ M. All electrochemical experiments were performed in 0.5 M KCl pH 6.00. The pH was adjusted to avoid the formation of other metal ion species, mainly hydroxides, in the solution aside from the free ion [65–67]. The selection of pH and an influence od electrolyte was previously described by the authors in review paper [68]. There was three well-defined peaks observed at anodic stripping voltammograms at –0.65 V, –0.44 V and –0.20 V confirming the presence of Cd^{2+}, Pb^{2+} and Cu^{2+} ion, respectively. Current intensities were multiplied by the dilution factor expressed by the equation (1):

$$DF = \frac{V_0 + V_s}{V_0} \ (1)$$

where V_0 is initial volume and V_s is the volume of added nanoparticles suspension in a particular portion.

3.3.1. Cd^{2+}, Pb^{2+}, Cu^{2+} ions binding by $Fe_3O_4@SiO_2$-cyclen - kinetics examination

First, kinetic studies were performed to determine the effectual time to establish the equilibrium in the solution after adding the nanoparticles portion. All voltammograms were recorded immediately after adding 1 mg of $Fe_3O_4@SiO_2$-cyclen nanoparticles to the ion solution and after every 5 minutes of having mixed the solution. In the graph is shown the actual time that the nanoparticles stayed in the solution due to the length of the DPASV measurement (Figure 5).

334
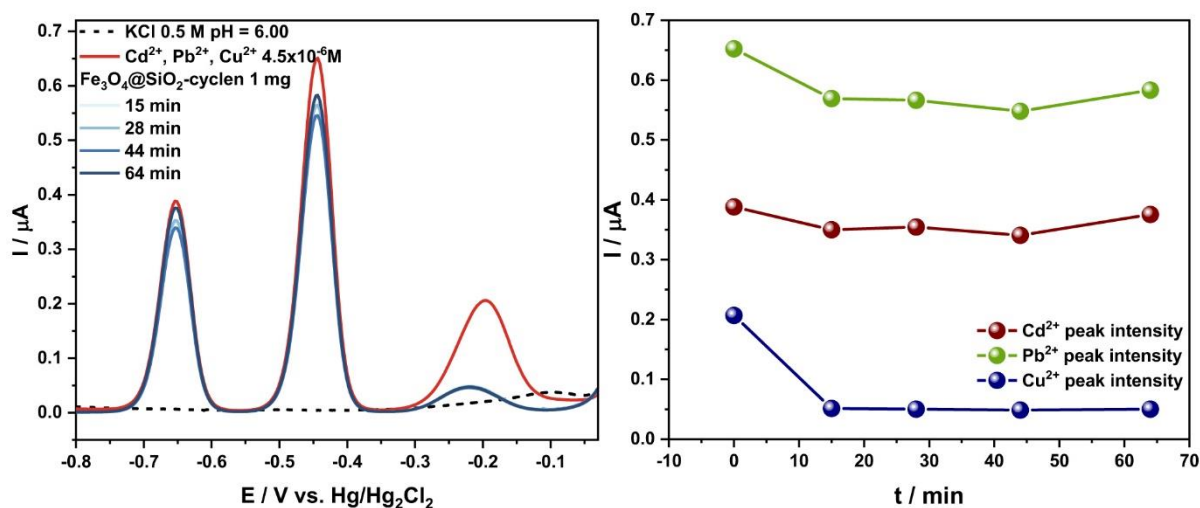
Figure 5. Simultaneous differential pulse anodic stripping voltammograms for examination of kinetics Cd^{2+}, Pb^{2+} and Cu^{2+} ($4.5 \cdot 10^{-6}$M) ions binding – changes of peak intensities over time after addition of 1 mg $Fe_3O_4@SiO_2$-cyclen nanoparticles.

After adding one portion of nanoparticles to the ion solution, a decrease in the peak intensity in the case of only the Cu^{2+} ion was observed. It can be stated that the addition 1 mg of nanoparticles does not affect $Cd^{2+}$and Pb^{2+} ions binding. It can be assumed that the slight peaks intensity changes are within the limit of the measurement error. On the basis of the experiment it can be concluded that the equilibrium in the solution is established no more than 15 minutes after adding the portion of nanoparticles. A different phenomenon is observed in the case of an experiment in independent Cd^{2+}, Pb^{2+} and Cu^{2+} ion solutions (Figure S1. in the Supporting Information file). In such a case, one observes a decrease in the peaks intensity over time for both the Cd^{2+} and Cu^{2+} ion after adding 0.5 mg $Fe_3O_4@SiO_2$- cyclen nanoparticles. Functionalised nanomagnetite show no tendency to Pb^{2+} ions binding and it is certainly not influenced by the time of their presence in the solution. It can be assumed that in the case of Cd^{2+} and Cu^{2+} ions the equilibrium in the solution is established after about 50 minutes after adding the nanoparticles. After analysing the kinetics of ion binding by $Fe_3O_4@SiO_2$- cyclen nanoparticles, both in individual ion solutions and simultaneous analysis, it was found that the optimal time for adding the nanoparticles portion to the solution to the measurement is 20 minutes after mixing. Also, the conducted kinetics experiment suggests that the ion binding level may be influenced by the amount of added nanoparticles. Consequently, the observed

355 dependencies lead to the study of the $Fe_3O_4@SiO_2$- cyclen nanoparticles binding capacity by

356 titration of the Cd^{2+}, Pb^{2+} and Cu^{2+} ions solution.

357

3.3.2. Determination of $Fe_3O_4@SiO_2$-cyclen binding ability in Cd^{2+}, Pb^{2+} and Cu^{2+} ions

359 **solutions**

360   In order to determine the ion Cd^{2+}, Pb^{2+} and Cu^{2+} binding capacity of

361 $Fe_3O_4@SiO_2$- cyclen nanoparticles, both in individual solutions and in the mixture, titration

362 with nanoparticles was performed. Used as the measurement analytical method was a two-stage

363 DPASV analysis involving pre-concentration and metal ions stripping. In the first stage, the

364 negative potential of –0.9 V was applied to Cd^{2+}, Pb^{2+} and Cu^{2+} ions electrodeposition on the

365 working electrode. Subsequently, the faradic current obtained by oxidation was recorded during

366 the potential sweep toward the positive potential direction from –0,8 V to –0.5 V, from –0,6 V

367 to –0.3 V, from –0,4 V to –0.04 V and from −0.8 V to 0.0 V, for Cd^{2+}, Pb^{2+}, Cu^{2+} and

368 simultaneous ions detection, respectively. A 0.25 mg portion of $Fe_3O_4@SiO_2$- cyclen

369 nanoparticles was added into ion solution at each titration step and mixed for 20 minutes before

370 starting the DPASV measurement. The mixing time was determined by the equilibrium

371 establishment experiment in time. Peaks intensity changes during the addition of further

372 nanoparticles portions were recalculated into sorption efficiency $R_\%$ (%) at every measuring

373 step based on the formula (2) [69]:

374 $$R_\% = \frac{(C_0 - C_f)}{C_0} \cdot 100\% \quad (2)$$

375 where C_0 (mg/L) is initial ion Me^{2+} concentration in the solution, C_f (C_e) (mg/L) is the final ion

376 concentration remaining in the solution [69].
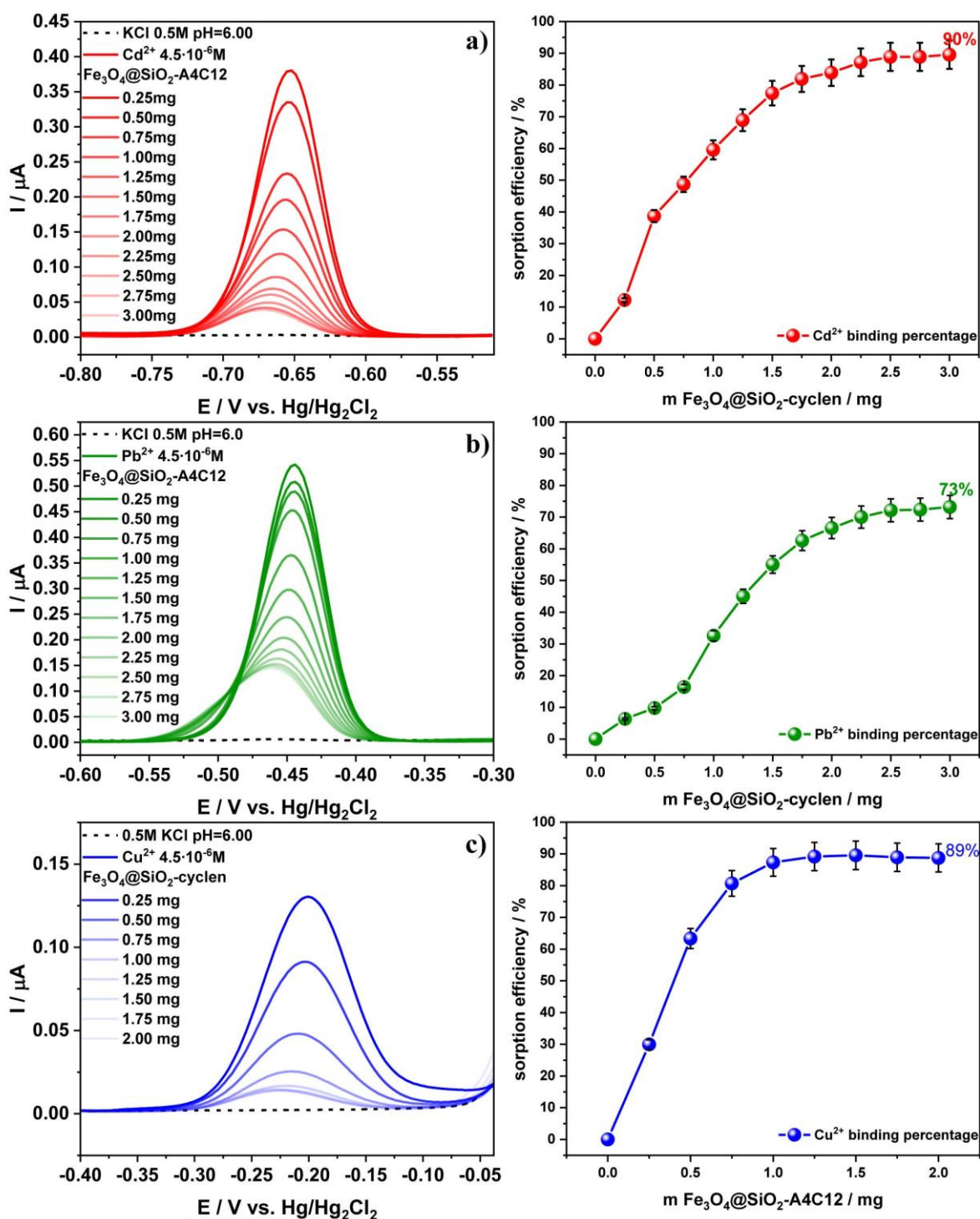
Figure 6. Individual differential pulse anodic stripping voltammograms and calculated sorption efficiency for a) Cd^{2+}, b) Pb^{2+} and c) Cu^{2+} ions binding by $Fe_3O_4@SiO_2$-cyclen nanoparticles.

Figure 6 shows an individual Cd^{2+}, Pb^{2+} and Cu^{2+} ions titration using $Fe_3O_4@SiO_2$- cyclen nanoparticles in portion of 0.25 mg added in every titration step. Figure 6 a) shows Cd^{2+} ions binding capacity. While adding successive nanoparticles portions,

the peak intensity decreases, thus the sorption efficiency increases. After adding about 2–2.5 mg of nanoparticles, the equilibrium is established and the next portions do not affect the peak intensity reduction. The sorption effectiveness reaches about 90% and remains at this level despite nanoparticles excess. A very similar phenomenon was observed during the titration of the Pb^{2+} ion (Figure 6b). Initially, the peak intensity decreases with each subsequent $Fe_3O_4@SiO_2$- cyclen portion so that after the addition of about 2–2.5 mg of nanoparticles, it reaches equilibrium. The titration ending determines the Pb^{2+} ion sorption efficiency at a level of 73%. The $Fe_3O_4@SiO_2$- cyclen nanoparticles behaviour was very different in the Cu^{2+} solution. Similar as in the case of Cd^{2+} and Pb^{2+} ions titrations, a decrease in peak intensity during titration was observed. However, a much smaller amount of nanoparticles was needed to establish equilibrium in the solution. An equilibrium establishing was observed after the addition of about 1 mg of nanoparticles. The addition of excess nanoparticles did not increase the sorption efficiency, and its level reached about 89%.

Afterwards, to compare, all three ions were titrated simultaneously by $Fe_3O_4@SiO_2$- cyclen nanoparticles starting with 0.25 mg for the first portion and 0.5 mg in the final steps (Figure 7).
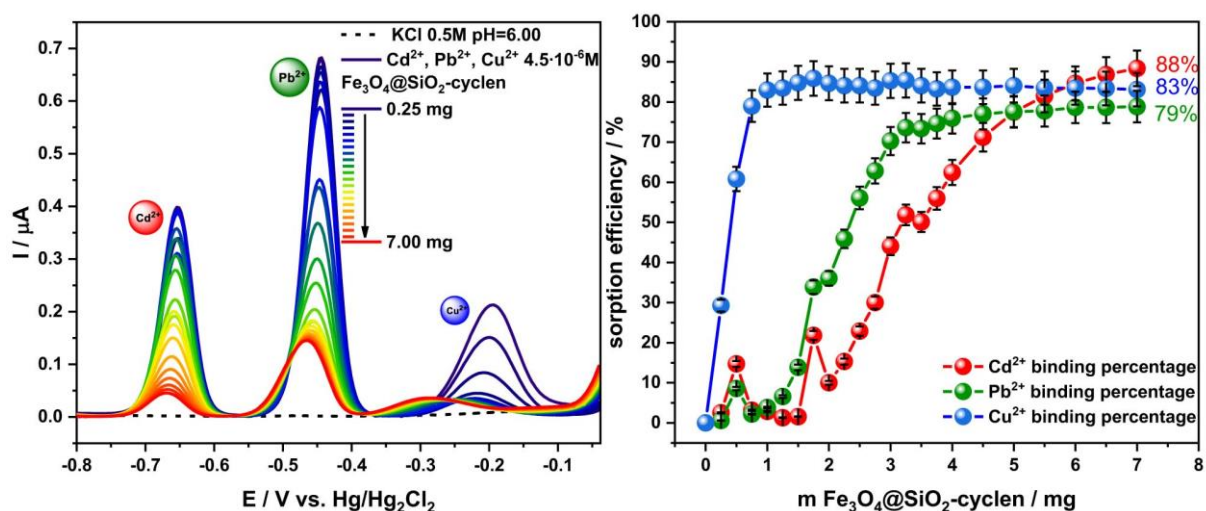
Figure 7. Simultaneous differential pulse anodic stripping voltammograms and calculated sorption efficiency for Cd^{2+}, Pb^{2+}, Cu^{2+} ions binding by $Fe_3O_4@SiO_2$-cyclen nanoparticles.

In the initial titration steps, only a decrease in the intensity of the Cu^{2+} peak was observed. After adding about 1–1.5 mg of nanoparticles, the percentage of Cu^{2+} binding remained unchanged at a level of 83%. Then, after the Cu^{2+} binding equilibrium establishing, changes in the intensity of the Cd^{2+} and Pb^{2+} peaks were observed. As more $Fe_3O_4@SiO_2$- cyclen portions are added, the intensity of the Cd^{2+} and Pb^{2+} peaks was reduced

and the binding efficiency increased. The Pb^{2+} binding equilibrium was established after adding about 3–3.5 mg of nanoparticles to the ions solution and the sorption efficiency reached 79%. As the last equilibrium was Cd^{2+} binding established after the addition stage of ion binding remains at a comparable level, however, it requires different amount of nanoparticles.

The exact calculated sorption efficiency parameters for individual (from Figure 6) and simultaneous (from Figure 7) is presented in Table 2. The sorption efficiency $R_{\%}$ calculated on the basis of the conducted DPASV experiments show that for Cd^{2+} this ion was detected at similar levels of 89-88% regardless as an individual ion in solution or in a mixture of studied ions. In the case of Pb^{2+}, the sorption level was higher for the simultaneous solution, while for Cu^{2+} sorption value was higher in the single-component. Nevertheless, the sorption efficiency are at very high levels for all analysed solutions, which confirms high efficiency of ions binding by $Fe_3O_4@SiO_2$-cyclen nanoparticles.

Table 2. Sorption efficiency parameters for individual and simultaneous Cd^{2+}, Pb^{2+} and Cu^{2+} ions binding by $Fe_3O_4@SiO_2$- cyclen nanoparticles.

	Individual	Simultaneous
	$R_{\%}$	$R_{\%}$
Cd^{2+}	89.55%	88.37%
Pb^{2+}	73.20%	78.85%
Cu^{2+}	88.75%	83.08%

3.3.3. Magnetic separation of adsorbed Cd^{2+}, Pb^{2+} and Cu^{2+}

Finally, the separation effectiveness of nanoparticles with adsorbed heavy metal ions by external magnetic field was investigated. First, the necessary amount of nanoparticles to bind Cd^{2+}, Pb^{2+}, Cu^{2+} ions solution was added to them. After that, the reduction in the metal ions peaks intensity at the DPAS voltammograms was observed (from blue line to yellow line). Then the nanoparticles contained in the solution were isolated with the use of a magnet and the solution was separated and subjected to DPASV measurement. The obtained voltammogram, apart from slightly negatively shifted potentials, shows no deviation from that obtained directly after the adsorption process. This phenomenon indicates the separation of all bound ions along with the nanoparticles from the solution (Figure 8).

434
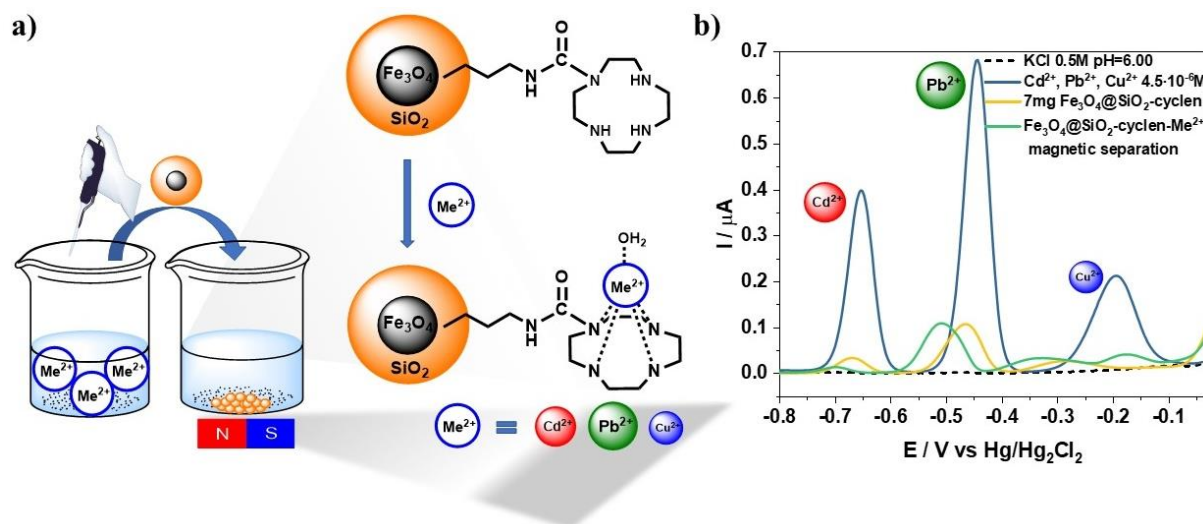
Figure 8. a) Scheme of magnetic Me^{2+} ions binding and magnetic separation experiment. Ion binding model by aza-crown based on Subat et al. [46]. b) Simultaneous differential pulse anodic stripping voltammograms: of Cd^{2+}, Pb^{2+}, Cu^{2+} ions (blue line), after adsorption by 7 mg $Fe_3O_4@SiO_2$-cyclen nanoparticles (yellow line) and after magnetic isolation nanoparticles with adsorbed ions (green line).

4. Conclusions

In this work, new core-shell nanostructures were synthesised containing a magnetic Fe_3O_4 core and silane shell functionalised with 1,4,7,10-tetraazacyclododecane were synthesised and characterised and their binding capacity was investigated. The results of nanomaterial characteristics using SEM, XPS, pXRD and FT-IR confirmed the success of the three-stage synthesis process.

Moreover, $Fe_3O_4@SiO_2$- cyclen nanoparticles binding kinetics and the sorption efficiency of Cd^{2+}, Pb^{2+} and Cu^{2+} was investigated both in individual ions solutions and in an ions mixture. Electrochemical studies proved that nanoparticles can be effectively used as adsorbents in environment heavy metal ions pollution management, which can be easily collected using an external magnetic field.

The research showed that nanoparticles have a binding tendency to all selected ions Cd^{2+}, Pb^{2+} and Cu^{2+} in their individual solutions and their sorption efficiency remains at 90%, 73% and 89%, respectively. It is worth mentioning that the smallest amount of nanoparticles was needed to bind the Cu^{2+}. Simultaneous Cd^{2+}, Pb^{2+} and Cu^{2+} determination also indicates the ability of $Fe_3O_4@SiO_2$-cyclen to bind of all ions. However, a clear order of ion binding was

observed in the mixture during the addition of further nanoparticles portions. First, Cu^{2+} ions were bound, then Pb^{2+} and Cd^{2+} the sorption efficiency remains at 83%, 79% and 88% level, respectively. This phenomenon can be explained by the complexation constants value of these ions by 1,4,7,10-tetraazacyclododecane. The fastest Cu^{2+} binding can be explained by the highest value of the complexation constant 23.9, 24.8 according to Antunes et al. [70], whereas the complexation constants of Pb^{2+} and Cd^{2+} are 15.9 and 14.3, respectively [70]. Additionally, the level of ion binding depends on the amount of added nanoparticles. On this basis, it can be concluded that the presence of cyclen functional groups on the surface of nanoparticles gives them the ability to bind ions. Furthermore, the Cd^{2+}, Pb^{2+}, Cu^{2+} ions adsorption and magnetic separation experiment confirms the effectiveness of ion binding and purification of water environments. On the basis of this work, it can be assumed that the new nanomaterials based on Fe_3O_4 and functionalised with N-(3-(triethoxysilyl)propyl)-1,4,7,10-tetraazacyclododecane-1-carboxamide can be successfully used as a universal Cd^{2+}, Pb^{2+}, Cu^{2+} ions magnetic adsorbent.

Acknowledgements

CRediT authorship contribution statement

Amanda Kulpa-Koterwa: Methodology, Formal analysis, Investigation, Data Curation, Writing - Original Draft, Writing - Review & Editing, Visualization, Funding acquisition **Jacek Ryl:** Investigation, Data Curation, Writing - Original Draft, **Karolina Górnicka:** Investigation, Data Curation, Writing - Original Draft **Paweł Niedziałkowski:** Conceptualization, Resources, Writing - Original Draft, Writing - Review & Editing, Supervision

Declaration of competing interest

The authors declare that they have no known competing financial interests or personal relationships that could have appeared to influence the work reported in this paper.

References

[1] S.S. Kolluru, S. Agarwal, S. Sireesha, I. Sreedhar, S.R. Kale, Heavy metal removal from wastewater using nanomaterials-process and engineering aspects, Process Safety and Environmental Protection. 150 (2021) 323–355. https://doi.org/10.1016/j.psep.2021.04.025.

[2] T.K. Das, A. Poater, Review on the Use of Heavy Metal Deposits from Water Treatment Waste towards Catalytic Chemical Syntheses, Int J Mol Sci. 22 (2021) 13383. https://doi.org/10.3390/ijms222413383.

[3] J. Briffa, E. Sinagra, R. Blundell, Heavy metal pollution in the environment and their toxicological effects on humans, Heliyon. 6 (2020) e04691. https://doi.org/10.1016/j.heliyon.2020.e04691.

[4] R.K. Gautam, S.K. Sharma, S. Mahiya, M.C. Chattopadhyaya, CHAPTER 1 Contamination of Heavy Metals in Aquatic Media: Transport, Toxicity and Technologies for Remediation, (2014) 1–24. https://doi.org/10.1039/9781782620174-00001.

[5] R. Shrestha, S. Ban, S. Devkota, S. Sharma, R. Joshi, A.P. Tiwari, H.Y. Kim, M.K. Joshi, Technological trends in heavy metals removal from industrial wastewater: A review, Journal of Environmental Chemical Engineering. 9 (2021) 105688. https://doi.org/10.1016/j.jece.2021.105688.

[6] D.-Q. Cao, X. Song, X.-M. Fang, W.-Y. Yang, X.-D. Hao, E. Iritani, N. Katagiri, Membrane filtration-based recovery of extracellular polymer substances from excess sludge and analysis of their heavy metal ion adsorption properties, Chemical Engineering Journal. 354 (2018) 866–874. https://doi.org/10.1016/j.cej.2018.08.121.

[7] A. Saeedi-Jurkuyeh, A.J. Jafari, R.R. Kalantary, A. Esrafili, A novel synthetic thin-film nanocomposite forward osmosis membrane modified by graphene oxide and polyethylene glycol for heavy metals removal from aqueous solutions, Reactive and Functional Polymers. 146 (2020) 104397. https://doi.org/10.1016/j.reactfunctpolym.2019.104397.

[8] Y. Ibrahim, E. Abdulkarem, V. Naddeo, F. Banat, S.W. Hasan, Synthesis of super hydrophilic cellulose-alpha zirconium phosphate ion exchange membrane via surface coating for the removal of heavy metals from wastewater, Science of The Total Environment. 690 (2019) 167–180. https://doi.org/10.1016/j.scitotenv.2019.07.009.

[9] S. Platzer, M. Kar, R. Leyma, S. Chib, A. Roller, F. Jirsa, R. Krachler, D.R. MacFarlane, W. Kandioller, B.K. Keppler, Task-specific thioglycolate ionic liquids for heavy metal extraction: Synthesis, extraction efficacies and recycling properties, Journal of Hazardous Materials. 324 (2017) 241–249. https://doi.org/10.1016/j.jhazmat.2016.10.054.

[10] Y. Deng, C. Feng, L. Tang, G. Zeng, Z. Chen, M. Zhang, Chapter 5 - Nanohybrid Photocatalysts for Heavy Metal Pollutant Control, in: L. Tang, Y. Deng, J. Wang, J. Wang, G. Zeng (Eds.), Nanohybrid and Nanoporous Materials for Aquatic Pollution Control, Elsevier, 2019: pp. 125–153. https://doi.org/10.1016/B978-0-12-814154-0.00005-0.

[11] X. Guan, X. Yuan, Y. Zhao, H. Wang, H. Wang, J. Bai, Y. Li, Application of functionalized layered double hydroxides for heavy metal removal: A review, Science of The Total Environment. (2022) 155693. https://doi.org/10.1016/j.scitotenv.2022.155693.

[12] C. Yan, Z. Qu, J. Wang, L. Cao, Q. Han, Microalgal bioremediation of heavy metal pollution in water: Recent advances, challenges, and prospects, Chemosphere. 286 (2022) 131870. https://doi.org/10.1016/j.chemosphere.2021.131870.

[13] J. He, J.P. Chen, A comprehensive review on biosorption of heavy metals by algal biomass: Materials, performances, chemistry, and modeling simulation tools,

535   Bioresource Technology. 160 (2014) 67–78.
536   https://doi.org/10.1016/j.biortech.2014.01.068.
537 [14] L. Yang, J. Wang, Y. Yang, S. Li, T. Wang, P. Oleksak, Z. Chrienova, Q. Wu, E.
538   Nepovimova, X. Zhang, K. Kuca, Phytoremediation of heavy metal pollution: Hotspots
539   and future prospects, Ecotoxicology and Environmental Safety. 234 (2022) 113403.
540   https://doi.org/10.1016/j.ecoenv.2022.113403.
541 [15] Q. Chen, Y. Yao, X. Li, J. Lu, J. Zhou, Z. Huang, Comparison of heavy metal removals
542   from aqueous solutions by chemical precipitation and characteristics of precipitates,
543   Journal of Water Process Engineering. 26 (2018) 289–300.
544   https://doi.org/10.1016/j.jwpe.2018.11.003.
545 [16] A.J. Bora, R.K. Dutta, Removal of metals (Pb, Cd, Cu, Cr, Ni, and Co) from drinking
546   water by oxidation-coagulation-absorption at optimized pH, Journal of Water Process
547   Engineering. 31 (2019) 100839. https://doi.org/10.1016/j.jwpe.2019.100839.
548 [17] A. Jain, S. Rai, R. Srinivas, R.I. Al-Raoush, Bioinspired modeling and biogeography-
549   based optimization of electrocoagulation parameters for enhanced heavy metal removal,
550   Journal of Cleaner Production. 338 (2022) 130622.
551   https://doi.org/10.1016/j.jclepro.2022.130622.
552 [18] S. Shukla, R. Khan, A. Daverey, Synthesis and characterization of magnetic
553   nanoparticles, and their applications in wastewater treatment: A review, Environmental
554   Technology & Innovation. 24 (2021) 101924. https://doi.org/10.1016/j.eti.2021.101924.
555 [19] R.M. Ali, H.A. Hamad, M.M. Hussein, G.F. Malash, Potential of using green adsorbent
556   of heavy metal removal from aqueous solutions: Adsorption kinetics, isotherm,
557   thermodynamic, mechanism and economic analysis, Ecological Engineering. 91 (2016)
558   317–332. https://doi.org/10.1016/j.ecoleng.2016.03.015.
559 [20] D. Saritha, A concise review on the removal of heavy metals from wastewater using
560   adsorbents, Materials Today: Proceedings. 63 (2022) 3973–3977.
561   https://doi.org/10.1016/j.matpr.2022.04.579.
562 [21] U. Haripriyan, K.P. Gopinath, J. Arun, Chitosan based nano adsorbents and its types for
563   heavy metal removal: A mini review, Materials Letters. 312 (2022) 131670.
564   https://doi.org/10.1016/j.matlet.2022.131670.
565 [22] I. Ihsanullah, M. Sajid, S. Khan, M. Bilal, Aerogel-based adsorbents as emerging
566   materials for the removal of heavy metals from water: Progress, challenges, and
567   prospects, Separation and Purification Technology. 291 (2022) 120923.
568   https://doi.org/10.1016/j.seppur.2022.120923.
569 [23] Y. Yue, Y. Liu, W. Zhang, J. Guo, Y. Gong, Y. Yu, Amidoxime functionalized low-cost
570   cellulose-based adsorbent derived from waste cigarette filters for efficient heavy metal
571   removal, Journal of Environmental Chemical Engineering. 10 (2022) 107846.
572   https://doi.org/10.1016/j.jece.2022.107846.
573 [24] H. Zhang, X. Hu, T. Li, Y. Zhang, H. Xu, Y. Sun, X. Gu, C. Gu, J. Luo, B. Gao, MIL
574   series of metal organic frameworks (MOFs) as novel adsorbents for heavy metals in
575   water: A review, Journal of Hazardous Materials. 429 (2022) 128271.
576   https://doi.org/10.1016/j.jhazmat.2022.128271.
577 [25] C. Duan, T. Ma, J. Wang, Y. Zhou, Removal of heavy metals from aqueous solution
578   using carbon-based adsorbents: A review, Journal of Water Process Engineering. 37
579   (2020) 101339. https://doi.org/10.1016/j.jwpe.2020.101339.
580 [26] S. Cho, J.-H. Kim, K.S. Yang, M. Chang, Facile preparation of amino-functionalized
581   polymeric microcapsules as efficient adsorbent for heavy metal ions removal, Chemical
582   Engineering Journal. 425 (2021) 130645. https://doi.org/10.1016/j.cej.2021.130645.
583 [27] E. Vunain, A. Mishra, B. Mamba, Dendrimers, mesoporous silicas and chitosan-based
584   nanosorbents for the removal of heavy-metal ions: A review, International Journal of

585 Biological Macromolecules. 86 (2016) 570–586.
586 https://doi.org/10.1016/j.ijbiomac.2016.02.005.

587 [28] M.M. Al-Mahadeen, A.G. Jiries, S.A. Al-Trawneh, S.F. Alshahateet, A.S. Eldouhaibi, S.
588 Sagadevan, Kinetics and equilibrium studies for the removal of heavy metal ions from
589 aqueous solution using the synthesized C-4-bromophenylcalix[4]resorcinarene
590 adsorbent, Chemical Physics Letters. 783 (2021) 139053.
591 https://doi.org/10.1016/j.cplett.2021.139053.

592 [29] Z. Cheng, J. Yang, L. Li, Y. Chen, X. Wang, Flocculation inspired combination of
593 layered double hydroxides and fulvic acid to form a novel composite adsorbent for the
594 simultaneous adsorption of anionic dye and heavy metals, Journal of Colloid and
595 Interface Science. 618 (2022) 386–398. https://doi.org/10.1016/j.jcis.2022.03.097.

596 [30] R. Torkaman, F. Maleki, M. Gholami, M. Torab-Mostaedi, M. Asadollahzadeh,
597 Assessing the radiation-induced graft polymeric adsorbents with emphasis on heavy
598 metals removing: A systematic literature review, Journal of Water Process Engineering.
599 44 (2021) 102371. https://doi.org/10.1016/j.jwpe.2021.102371.

600 [31] V. Vinayagam, S. Murugan, R. Kumaresan, M. Narayanan, M. Sillanpää, D.-V.N. Vo,
601 O.S. Kushwaha, Protein nanofibrils as versatile and sustainable adsorbents for an
602 effective removal of heavy metals from wastewater: A review, Chemosphere. 301 (2022)
603 134635. https://doi.org/10.1016/j.chemosphere.2022.134635.

604 [32] J. R., B. Gurunathan, S. K, S. Varjani, H.H. Ngo, E. Gnansounou, Advancements in
605 heavy metals removal from effluents employing nano-adsorbents: Way towards cleaner
606 production, Environmental Research. 203 (2022) 111815.
607 https://doi.org/10.1016/j.envres.2021.111815.

608 [33] R. Bhateria, R. Singh, A review on nanotechnological application of magnetic iron
609 oxides for heavy metal removal, Journal of Water Process Engineering. 31 (2019)
610 100845. https://doi.org/10.1016/j.jwpe.2019.100845.

611 [34] A. Latif, D. Sheng, K. Sun, Y. Si, M. Azeem, A. Abbas, M. Bilal, Remediation of heavy
612 metals polluted environment using Fe-based nanoparticles: Mechanisms, influencing
613 factors, and environmental implications, Environmental Pollution. 264 (2020) 114728.
614 https://doi.org/10.1016/j.envpol.2020.114728.

615 [35] F. Ghorbani, S. Kamari, Core–shell magnetic nanocomposite of Fe3O4@SiO2@NH2 as
616 an efficient and highly recyclable adsorbent of methyl red dye from aqueous
617 environments, Environmental Technology & Innovation. 14 (2019) 100333.
618 https://doi.org/10.1016/j.eti.2019.100333.

619 [36] S. Patil, R. Tandon, N. Tandon, A current research on silica coated ferrite nanoparticle
620 and their application: Review, Current Research in Green and Sustainable Chemistry. 4
621 (2021) 100063. https://doi.org/10.1016/j.crgsc.2021.100063.

622 [37] L. Wang, X. Huang, C. Wang, X. Tian, X. Chang, Y. Ren, S. Yu, Applications of
623 surface functionalized Fe3O4 NPs-based detection methods in food safety, Food
624 Chemistry. 342 (2021) 128343. https://doi.org/10.1016/j.foodchem.2020.128343.

625 [38] S. Jin, B.C. Park, W.S. Ham, L. Pan, Y.K. Kim, Effect of the magnetic core size of
626 amino-functionalized Fe3O4-mesoporous SiO2 core-shell nanoparticles on the removal
627 of heavy metal ions, Colloids and Surfaces A: Physicochemical and Engineering
628 Aspects. 531 (2017) 133–140. https://doi.org/10.1016/j.colsurfa.2017.07.086.

629 [39] Y. Harinath, D.H.K. Reddy, L.S. Sharma, K. Seshaiah, Development of hyperbranched
630 polymer encapsulated magnetic adsorbent (Fe3O4@SiO2–NH2-PAA) and its
631 application for decontamination of heavy metal ions, Journal of Environmental Chemical
632 Engineering. 5 (2017) 4994–5001. https://doi.org/10.1016/j.jece.2017.09.031.

633 [40] N. Naini, H. Sid Kalal, M.R. Almasian, D. Niknafs, M. Taghiof, H. Hoveidi, Phosphine-
634 functionalized Fe3O4/SiO2/composites as efficient magnetic nanoadsorbents for the

635   removal of palladium ions from aqueous solution: Kinetic, thermodynamic and isotherm
636   studies, Materials Chemistry and Physics. 287 (2022) 126242.
637   https://doi.org/10.1016/j.matchemphys.2022.126242.

638 [41] E. Ragheb, M. Shamsipur, F. Jalali, F. Mousavi, Modified magnetic-metal organic
639   framework as a green and efficient adsorbent for removal of heavy metals, Journal of
640   Environmental Chemical Engineering. 10 (2022) 107297.
641   https://doi.org/10.1016/j.jece.2022.107297.

642 [42] W. Qin, S. Xu, G. Xu, Q. Xie, C. Wang, Z. Xu, Preparation of silica gel bound crown
643   ether and its extraction performance towards zirconium and hafnium, Chemical
644   Engineering Journal. 225 (2013) 528–534. https://doi.org/10.1016/j.cej.2013.03.127.

645 [43] M. Subat, K. Woinaroschy, S. Anthofer, B. Malterer, B. König, 1,4,7,10-
646   Tetraazacyclododecane Metal Complexes as Potent Promoters of Carboxyester
647   Hydrolysis under Physiological Conditions, Inorg. Chem. 46 (2007) 4336–4356.
648   https://doi.org/10.1021/ic070101z.

649 [44] J.M. Park, O.J. Shon, H. Hong, J.S. Kim, Y. Kim, H.B. Lim, Development of a
650   microchip metal ion sensor using dinitro-azocalix[4]azacrown, Microchemical Journal.
651   80 (2005) 139–144. https://doi.org/10.1016/j.microc.2004.07.017.

652 [45] B. König, M. Pelka, M. Subat, I. Dix, P.G. Jones, Urea Derivatives of 1,4,7,10-
653   Tetraazacyclododecane − Synthesis and Binding Properties, European Journal of
654   Organic Chemistry. 2001 (2001) 1943–1949. https://doi.org/10.1002/1099-
655   0690(200105)2001:10<1943::AID-EJOC1943>3.0.CO;2-O.

656 [46] M. Subat, K. Woinaroschy, C. Gerstl, B. Sarkar, W. Kaim, B. König, 1,4,7,10-
657   Tetraazacyclododecane Metal Complexes as Potent Promoters of Phosphodiester
658   Hydrolysis under Physiological Conditions, Inorg. Chem. 47 (2008) 4661–4668.
659   https://doi.org/10.1021/ic702413q.

660 [47] M. Regueiro-Figueroa, E. Ruscsák, L. Fra, G. Tircsó, I. Tóth, A. de Blas, T. Rodríguez-
661   Blas, C. Platas-Iglesias, D. Esteban-Gómez, Highly Stable Complexes of Divalent Metal
662   Ions (Mg^{2+}, Ca^{2+}, Cu^{2+}, Zn^{2+}, Cd^{2+}, and Pb^{2+}) with a Dota-Like Ligand Containing
663   a Picolinate Pendant, European Journal of Inorganic Chemistry. 2014 (2014) 6165–6173.
664   https://doi.org/10.1002/ejic.201402693.

665 [48] P. Antunes, P.M. Campello, R. Delgado, M.G.B. Drew, V. Félix, I. Santos, Metal
666   complexes of a tetraazacyclophane: solution and molecular modelling studies, Dalton
667   Trans. (2003) 1852–1860. https://doi.org/10.1039/B301033C.

668 [49] P. Niedziałkowski, D. Zarzeczańska, T. Ossowski, Synthesis and Characterization of
669   1,4,7,10-Tetraazacyclododecane Derivatives and Their Metal Complexes, Polish Journal
670   of Chemistry. Vol. 82 (2008) 1175–1197.

671 [50] A. Kulpa, J. Ryl, G. Skowierzak, A. Koterwa, G. Schroeder, T. Ossowski, P.
672   Niedziałkowski, Comparison of Cadmium Cd^{2+} and Lead Pb^{2+} Binding by
673   Fe2O3@SiO2-EDTA Nanoparticles – Binding Stability and Kinetic Studies,
674   Electroanalysis. 32 (2020) 588–597. https://doi.org/10.1002/elan.201900616.

675 [51] A. Kulpa, J. Ryl, G. Schroeder, A. Koterwa, J. Sein Anand, T. Ossowski, P.
676   Niedziałkowski, Simultaneous voltammetric determination of Cd^{2+}, Pb^{2+}, and Cu^{2+}
677   ions captured by Fe3O4@SiO2 core-shell nanostructures of various outer amino chain
678   length, Journal of Molecular Liquids. 314 (2020) 113677.
679   https://doi.org/10.1016/j.molliq.2020.113677.

680 [52] S. Sawan, R. Maalouf, A. Errachid, N. Jaffrezic-Renault, Metal and metal oxide
681   nanoparticles in the voltammetric detection of heavy metals: A review, TrAC Trends in
682   Analytical Chemistry. 131 (2020) 116014. https://doi.org/10.1016/j.trac.2020.116014.

[53] T. Matsuoka, S. Yamamoto, O. Moriya, M. Kashio, T. Sugizaki, Synthesis of thermoresponsive polysilsesquioxane with methoxyethylamide group and crown ether, Polym J. 42 (2010) 313–318. https://doi.org/10.1038/pj.2010.7.

[54] M.C. Biesinger, B.P. Payne, A.P. Grosvenor, L.W.M. Lau, A.R. Gerson, R.St.C. Smart, Resolving surface chemical states in XPS analysis of first row transition metals, oxides and hydroxides: Cr, Mn, Fe, Co and Ni, Applied Surface Science. 257 (2011) 2717– 2730. https://doi.org/10.1016/j.apsusc.2010.10.051.

[55] Š. Meškinis, A. Vasiliauskas, M. Andrulevičius, D. Peckus, S. Tamulevičius, K. Viskontas, Diamond Like Carbon Films Containing Si: Structure and Nonlinear Optical Properties, Materials. 13 (2020) 1003. https://doi.org/10.3390/ma13041003.

[56] F. Sirotti, M. De Santis, G. Rossi, Synchrotron-radiation photoemission and x-ray absorption of Fe silicides, Phys. Rev. B. 48 (1993) 8299–8306. https://doi.org/10.1103/PhysRevB.48.8299.

[57] R. Bywalez, H. Karacuban, H. Nienhaus, C. Schulz, H. Wiggers, Stabilization of mid-sized silicon nanoparticles by functionalization with acrylic acid, Nanoscale Research Letters. 7 (2012) 76. https://doi.org/10.1186/1556-276X-7-76.

[58] A. Mohtasebi, T. Chowdhury, L.H.H. Hsu, M.C. Biesinger, P. Kruse, Interfacial Charge Transfer between Phenyl-Capped Aniline Tetramer Films and Iron Oxide Surfaces, J. Phys. Chem. C. 120 (2016) 29248–29263. https://doi.org/10.1021/acs.jpcc.6b09950.

[59] A. Tanver, M.-H. Huang, Y. Luo, Energetic interpenetrating polymer network (EIPN): enhanced thermo-mechanical properties of NCO-fMWCNTs/HTPB PU and alkyne-fMWCNTs/acyl-GAP based nanocomposite and its propellants, RSC Adv. 6 (2016) 49101–49112. https://doi.org/10.1039/C6RA07742K.

[60] Q. Li, C.W. Kartikowati, S. Horie, T. Ogi, T. Iwaki, K. Okuyama, Correlation between particle size/domain structure and magnetic properties of highly crystalline Fe3O4 nanoparticles, Sci Rep. 7 (2017) 9894. https://doi.org/10.1038/s41598-017-09897-5.

[61] F. Shalali, S. Cheraghi, M.A. Taher, A sensitive electrochemical sensor amplified with ionic liquid and N-CQD/Fe3O4 nanoparticles for detection of raloxifene in the presence of tamoxifen as two essentials anticancer drugs, Materials Chemistry and Physics. 278 (2022) 125658. https://doi.org/10.1016/j.matchemphys.2021.125658.

[62] T. Yousofi, A. Rahmati, Fe3O4@SiO2-BU core-shell as a new nanomagnetic gelator for oil recovery from water, Polyhedron. 180 (2020) 114363. https://doi.org/10.1016/j.poly.2020.114363.

[63] T. Akbarpour, J. Yousefi Seyf, A. Khazaei, N. Sarmasti, Synthesis of Pyrano [2,3-c] Pyrazole Derivatives Using a Novel Ionic-Liquid Based Nano-Magnetic Catalyst (Fe 3 O 4 @SiO 2 @(CH 2) 3 NH@CC@Imidazole@SO 3 H + Cl −), Polycyclic Aromatic Compounds. (2021) 1–21. https://doi.org/10.1080/10406638.2021.1873152.

[64] D. Chen, T. Awut, B. Liu, Y. Ma, T. Wang, I. Nurulla, Functionalized magnetic Fe3O4 nanoparticles for removal of heavy metal ions from aqueous solutions, E-Polymers. 16 (2016) 313–322. https://doi.org/10.1515/epoly-2016-0043.

[65] Q. Kong, C. Wei, S. Preis, Y. Hu, F. Wang, Facile preparation of nitrogen and sulfur co-doped graphene-based aerogel for simultaneous removal of Cd2+ and organic dyes, Environ Sci Pollut Res Int. 25 (2018) 21164–21175. https://doi.org/10.1007/s11356-018-2195-8.

[66] T. Chen, H. Li, H. Wang, X. Zou, H. Liu, D. Chen, Y. Zhou, Removal of Pb(II) from Aqueous Solutions by Periclase/Calcite Nanocomposites, Water Air Soil Pollut. 230 (2019) 299. https://doi.org/10.1007/s11270-019-4354-z.

[67] J. Liu, D. Luo, L. Huang, Y. Wang, S. Wen, Copper adsorption reaction rate and ion exchange ratio during the copper activation of sphalerite, Physicochem. Probl. Miner. Process. 54 (2017) 377–385. https://doi.org/10.5277/ppmp1832.

733   [68] A. Kulpa-Koterwa, T. Ossowski, P. Niedziałkowski, Functionalized Fe3O4
734   Nanoparticles as Glassy Carbon Electrode Modifiers for Heavy Metal Ions
735   Detection—A Mini Review, Materials. 14 (2021) 7725.
736   https://doi.org/10.3390/ma14247725.
737   [69] C. Zeng, P. Liu, Z. Xiao, Y. Li, L. Song, Z. Cao, D. Wu, Y.-F. Zhang, Highly Selective
738   Adsorption and Recovery of Palladium from Spent Catalyst Wastewater by 1,4,7,10-
739   Tetraazacyclododecane-Modified Mesoporous Silica, ACS Sustainable Chem. Eng. 10
740   (2022) 1103–1114. https://doi.org/10.1021/acssuschemeng.1c05915.
741   [70] P. Antunes, P.M. Campello, R. Delgado, M.G.B. Drew, V. Félix, I. Santos, Metal
742   complexes of a tetraazacyclophane: solution and molecular modelling studies, Dalton
743   Trans. (2003) 1852–1860. https://doi.org/10.1039/B301033C.
744